Inorg. Chem. **2004**, *43*, 6633–6639

Magnetic Ordering in Iron Tricyanomethanide

Ralf Feyerherm,*,† Anja Loose,† Sven Landsgesell,† and Jamie L. Manson*,‡

Hahn-Meitner-Institute and Berlin Neutron Scattering Center, Department SF2, Glienicker Strasse 100, 14109 Berlin, Germany, and Department of Chemistry and Biochemistry, 226 Science Building, Eastern Washington University, Cheney, Washington 99004-2440

Received May 4, 2004

Magnetic susceptibility, heat capacity, and neutron diffraction studies of $Fe[C(CN)_3]_2$ reveal the existence of two magnetic phase transitions at $T_{N,I} = 2.45$ K and $T_{N,II} = 1.85$ K. Between 1.85 and 2.45 K, the magnetic ordering is incommensurate with a temperature-dependent propagation vector ($k_{I,x}$ 0 0), $k_{I,x} = 0.525$–0.540. In zero magnetic field, below 1.85 K the ordered structure is described by the propagation vector $k_{II} = (^1/_2\ 0\ ^1/_2)$, i.e., a doubling of the unit cell along the *a* and *c* directions of the orthorhombic lattice. The ordered moments of 3.4(1) and 3.2(1) μ_B, respectively, are aligned approximately parallel to the principal axis of the elongated Fe coordination octahedron. At $T < T_{N,II}$, application of an external magnetic field of about 18 kOe destroys the commensurate phase and the incommensurate phase is established. The latter phase is stable in fields up to about 40 kOe. The magnetic ordering of $Fe[C(CN)_3]_2$ is discussed in terms of the 2D triangular topology of the lattice, producing partial frustration, and in comparison with the behavior of other compounds of the series $M[C(CN)_3]_2$, where M is a 3d transition metal.

Introduction

A number of organic ligands have been shown to be able to provide magnetic superexchange pathways between transition metal ions leading to a class of molecule-based magnetic materials.[1] In the large majority of published work, bidentate ligands are employed, which already result in a variety of interesting magnetic ground states related to different structural topologies, like oligomers, chains, and two- and three-dimensional networks.

Tridentate ligands, in turn, are rare. However, they are expected to add another flavor to magnetism in molecule-based compounds, because they may give rise to new topologies, like triangular magnetically frustrated lattices. Recently, the synthesis and magnetic properties of the series $M[C(CN)_3]_2$, with M = 3d transition metal, has been reported,[2−6] where the tricyanomethanide anion, $C(CN)_3^-$, has 3-fold symmetry. It has been shown[7] that the magnetic topology of these compounds is that of a two-dimensional (2D) distorted triangular lattice represented by the "row model" introduced by Kawamura[8] and Zhang et al.[9] This model describes a lattice of equal-legged triangles, with a different magnetic interaction along rows of M ions than between the rows, leading to a partial lifting of frustration.

To date, only in $Cr[C(CN)_3]_2$ and $Mn[C(CN)_3]_2$ has long-range magnetic ordering been observed and studied by neutron diffraction.[5,7] No ordering above 2 K was observed in $V[C(CN)_3]_2$[5] as well as the Cu, Ni, and Co compounds.[4,6] Although frustration effects appear to reduce the ordering temperature in $Cr[C(CN)_3]_2$, the partial lifting of frustration in the row model in conjunction with Ising behavior results in a rather conventional magnetically ordered structure below $T_N = 6.1$ K in this compound, involving doublings of the unit cell along two crystal axes.[5] In contrast, $Mn[C(CN)_3]_2$ exhibits an incommensurate spiral magnetically ordered

* Authors to whom correspondence should be addressed. E-mail: feyerherm@hmi.de (R.F.); jmanson@ewu.edu (J.L.M.). Phone: ++49 30 8062 3082 (R.F.); (509) 359-2878 (J.L.M.). Fax: ++49 30 8062 3172 (R.F.); (509) 359-6973 (J.L.M.).

† Hahn-Meitner-Institute and Berlin Neutron Scattering Center.

‡ Eastern Washington University.

(1) Kahn, O. Molecular Magnetism; VCH: New York, 1993. Miller, J. S.; Epstein, A. *Angew. Chem., Int. Ed. Engl.* **1994**, *33*, 385. Gatteschi, D. *Adv. Mater.* **1994**, *6*, 635.
(2) Batten, S. R.; Hoskins, B. F.; Robson, R. *J. Chem. Soc., Chem. Commun.* **1991**, 445.
(3) Manson, J. L.; Campana, C.; Miller, J. S. *Chem. Commun.* **1998**, 251.
(4) Hoshio, H.; Iida, K.; Kawamoto, T.; Mori, T. *Inorg. Chem.* **1998**, *38*, 4229.
(5) Manson, J. L.; Ressouche, E.; Miller, J. S. *Inorg. Chem.* **2000**, *39*, 1135.
(6) Kurmoo, M. *Mol. Cryst. Liq. Cryst.* **2000**, *342*, 167.
(7) Feyerherm, R.; Loose, A.; Manson, J. L. *J. Phys.: Condens. Matter* **2003**, *15*, 663. Erratum: *J. Phys.: Condens. Matter* **2003**, *15*, 6057.
(8) Kawamura, H. *Prog. Theor. Phys. Suppl.* **1990**, *101*, 545.
(9) Zhang, W.; Saslow, W. M.; Gaby, M. *Phys. Rev. B* **1991**, *44*, 5129.

10.1021/ic049423i CCC: $27.50 © 2004 American Chemical Society
Published on Web 09/14/2004

structure below $T_N = 1.18$ K typical for a Heisenberg spin system on a partially frustrated triangular lattice.[7]

Here, we report on magnetization, heat capacity, and neutron diffraction studies of $Fe[C(CN)_3]_2$ which reveal two phase transitions at 1.85 and 2.45 K, corresponding to two different long-range magnetically ordered phases, one of which is incommensurate. The temperature and magnetic-field dependence of these phases is studied in detail by neutron diffraction.

Experimental Section

A microcrystalline, pale green sample of $Fe[C(CN)_3]_2$ resulted from the fast precipitation from an aqueous solution of $K[C(CN)_3]_2$ and $FeCl_2$. The sample was filtered, washed with H_2O, and dried under vacuum. The neutron powder diffraction data discussed in detail below characterize the sample as phase pure with no indication for a secondary phase down to the 5% level and show that $Fe[C(CN)_3]_2$ is isostructural to the other compounds of the series $M[C(CN)_3]_2$.

Magnetization measurements were carried out using an MPMS Squid magnetometer (Quantum Design). Some 20 mg of sample was loaded to a gelatin capsule attached to a plastic straw. The raw data were corrected for a diamagnetic contribution determined experimentally as described in the next section.

Heat capacity measurements were conducted using an Oxford Instrument 9 T MagLab calorimeter with ^{3}He refrigerator. Since no bulk specimens of $Fe[C(CN)_3]_2$ are available, a 1:3 mixture of the powder sample and grease containing alumina powder (Wakefield 120-2) was produced and a very small amount of the mixture ($\sim$1 mg) attached to the sapphire chip which is the central part of the calorimeter. The data obtained in this way are analyzed only qualitatively, basically to identify the phase transition temperatures.

Neutron powder diffraction measurements were performed using the instruments V1 and E9 at the Berlin Neutron Scattering Center (BENSC). Some 1.5 g of sample was filled into a vanadium can (7 mm diameter). Neutron wavelengths of 4.513 and 1.7964 Å, respectively, were used. The instrument V1 provides a high neutron flux and medium resolution, is equipped with a two-dimensional area detector, and covers a range of scattering angles up to about 100°. The data from the area detector are integrated over equal values of 2θ. In contrast to V1, the instrument E9 is a low-flux high-resolution powder diffractometer with an extended 2θ range up to 160°. Therefore, the former was used for the study of magnetic Bragg reflections, while the latter was used for the crystal structure determination. Magnetic-field-dependent measurements were carried out by using the horizontal-field superconducting cryomagnet HM-2 providing a maximum field of 40 kOe. The Rietveld refinement of the diffraction data was carried out using the WINPLOTR/FULLPROF package.[10]

Results

Crystal Structure. Like the other members of the series $M[C(CN)_3]_2$ (M = 3d transition metal), $Fe[C(CN)_3]_2$ crystallizes in an orthorhombic lattice, space group *Pmna*. Figure 1 shows the high-resolution neutron diffraction data taken at 1.5 and 5 K together with the Rietveld refinement of the corresponding structural model. The structural parameters are listed in detail in Table 1. In the 1.5 K diffractogram a few additional Bragg reflections can be identified that are absent at 5 K, the most significant one located at $2\theta = 8.4°$. As discussed in detail below, this is related to magnetic ordering appearing below 2.5 K in $Fe[C(CN)_3]_2$. For the Rietveld refinement of the 1.5 K data, the magnetic structure model described below has been taken into account. Within the experimental errors the crystal structure parameters do not change between 1.5 and 5 K.

The structural topology of the $M[C(CN)_3]_2$ series has been discussed in great detail previously.[2−7] The crystal structure consists of two identical interpenetrating three-dimensional rutilelike networks separated along *b* by one lattice unit; i.e.,

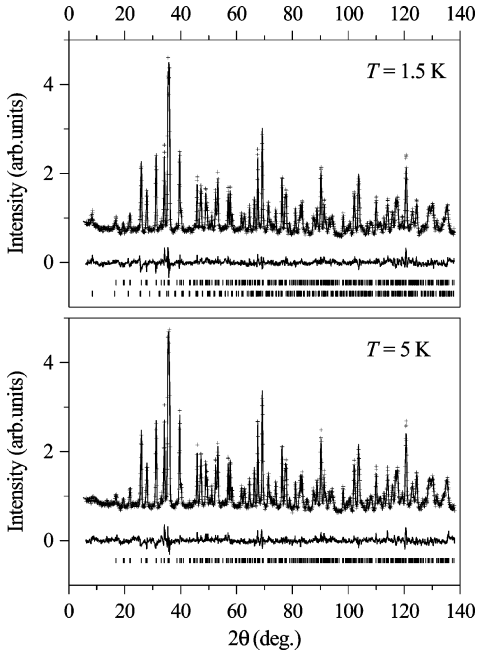

Figure 1. High-resolution neutron diffraction data (+) taken at 1.5 and 5 K together with the Rietveld refinement of the corresponding structural model (solid line through the data) and the residual (solid line at the bottom). Vertical bars at the bottom mark the positions of allowed Bragg reflections—for the 1.5 K data the magnetically ordered phase was taken into account. The neutron wavelength was 1.7964 Å.

Table 1. Crystal Structure Parameters from the Rietveld Refinement of High-Resolution Neutron Diffraction Data[a]

atom	mult	*x*/*a*	*y*/*b*	*z*/*c*	B_{iso} (Å^2)
			$T = 1.5$ K[b]		
Fe	2*c*	0	1/2	1/2	0.17(9)
N1	8*i*	0.2108(7)	0.2810(11)	0.5780(5)	0.23(4)
N2	4*h*	1/2	−0.2714(16)	0.8270(7)	0.23
C1	8*i*	0.3412(10)	0.1896(14)	0.6157(8)	0.18(5)
C2	4*h*	1/2	0.0835(19)	0.6592(10)	0.18
C3	4*h*	1/2	−0.1169(22)	0.7516(11)	0.18
			$T = 5$ K[c]		
Fe	2*c*	0	1/2	1/2	0.21(9)
N1	8*i*	0.2111(7)	0.2809(11)	0.5780(5)	0.23(4)
N2	4*h*	1/2	−0.2729(16)	0.8267(7)	0.23
C1	8*i*	0.3415(10)	0.1894(14)	0.6157(8)	0.26(5)
C2	4*h*	1/2	0.0834(19)	0.6597(10)	0.26
C3	4*h*	1/2	−0.1170(21)	0.7518(11)	0.26

[a] Mult: multiplicity and Wykoff letter. $R_{Bragg} = \Sigma|I_{obs} - I_{calc}|/\Sigma I_{obs}$, where *I* refers to the intensities of the Bragg reflections. $B_{iso} = 8\pi^2 <u^2>$, where $<u^2>$ is the mean square displacement. The other *R* values are $R_p = 0.041$ (0.041), $R_{wp} = 0.051$ (0.052), and $R_{exp} = 0.033$ (0.031) for the 1.5 K (5 K) data. [b] *Pmna*, $a = 7.5371(3)$ Å, $b = 5.3005(3)$ Å, $c = 10.4636(5)$ Å, and $R_{Bragg} = 0.063$. [c] *Pmna*, $a = 7.5374(3)$ Å, $b = 5.3004(3)$ Å, $c = 10.4638(5)$ Å, and $R_{Bragg} = 0.067$.

(10) Roisnel, T.; Rodríguez-Carvajal, J. *Mater. Sci. Forum* **2001**, *378−381*, 118.

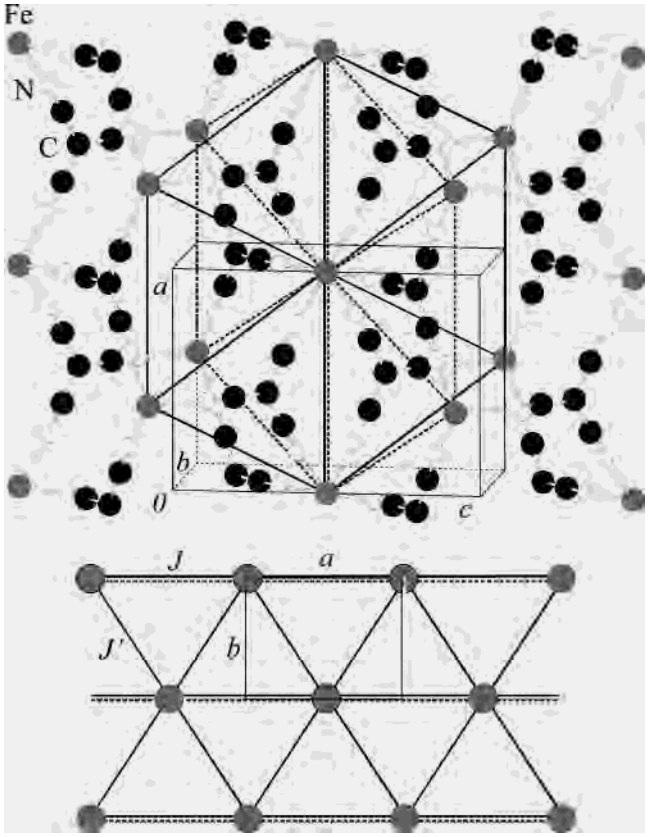

Figure 2. Top: Crystal structure of Fe[C(CN)$_3$]$_2$. Two triangular sheets intersecting at a row parallel to *a* are marked. For clarity, only one of the two identical interpenetrating networks is shown. The second network is shifted along b by one lattice unit. Bottom: Projection of the Fe sublattice onto the *ab* plane showing the magnetic topology with two different exchange pathways *J* and *J*′.

atoms at y and $(y + 1)$ belong to different networks. As depicted in Figure 2, each network is built of triangular sheets that intersect at rows parallel to *a*. In the related Mn-[C(CN)3]2 compound this structural motif results in partial frustration and a corresponding spiral magnetically ordered structure.[7] In Fe[C(CN)$_3$]$_2$, the Fe is located within an elongated octahedron with the N1 atoms forming the equatorial plane ($d_{Fe-N1} = 2.132$ Å) and the N2 at the apical positions ($d_{Fe-N2} = 2.176$ Å). The principal axis of the octahedron is tilted from the *c* axis by 37° toward *b*.

Magnetic Susceptibility. Figure 3 shows the temperature dependence of the magnetic susceptibility χ between 1.8 and 300 K measured for an applied field of $H = 1$ kOe. The raw data were fitted to a modified Curie−Weiss equation $\chi = C/(T - \Theta) + \chi_0$ in the temperature range 50−300 K resulting in $C = 3.27(1)$ emu K mol^{-1} and $\Theta = -7.0(1)$ K. The diamagnetic contribution from the sample and the capsule, $\chi_0 = 2.1 \times 10^{-4}$ emu mol^{-1}, was subtracted. The C value is consistent with the expected $S = 2$ high-spin state of the Fe^{2+} ions. The negative value of Θ is indicative of antiferromagnetic interactions between the Fe magnetic moments.

Alternatively, the data between 10 and 300 K were fitted to the high-temperature series expansion,

$$\chi(T) - \chi_0 = \frac{C}{T}(1 + \sum_{n=1}^{\infty} a_n K^n)$$

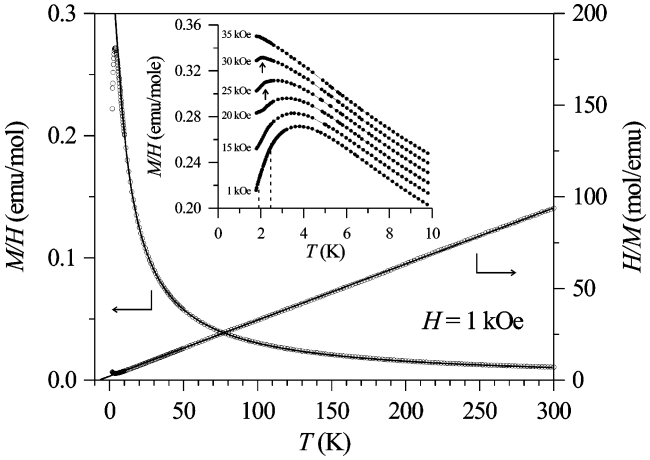

Figure 3. Temperature dependence of the magnetic susceptibility. The solid line through the H/M curve in the main plot is the fit to the Curie−Weiss law, and the line through the M/H curve, the fit to the high-temperature series expansion for the $S = 2$ 2D triangular Ising model; the see text. The inset shows low-temperature data measured for various values of the magnetic field (for clarity the curves were shifted upward to be separated by 0.01 emu/mol units each). The zero-field magnetic transition temperatures, as determined from the neutron diffraction experiment, are marked by the dashed vertical lines. In the susceptibility data, these transitions are hard to identify. Only for $H = 25$ and 30 kOe, antiferromagnetic transitions can be located as marked by arrows.

where $K = J^*/k_BT$, (a) for the S = 2 2D plane triangular Ising model,

$$\mathbf{H} = -\sum_{i,j} J^* S_i^z \cdot S_j^z$$

with coefficients a_n taken from ref 11 and (b) for the respective Heisenberg model,

$$\mathbf{H} = -\sum_{i,j} J^{**} \vec{S}_i \cdot \vec{S}_j$$

with coefficients an from ref 12. Both fits were of similar good quality and resulted in $C = 3.22(1)$ emu K mol^{-1}, $J^*/k_B = -0.240(5)$ K, and $J^{**}/k_B = -0.228(5)$ K, respectively. These values may be taken as estimate of the average value, $(J + 2J')/3$, of the two exchange parameters *J* and *J*′ in the present magnetic topology.

On cooling of the sample below 10 K, the magnetic susceptibility deviates from the divergent behavior extrapolated from the high-temperature series expansion results. It exhibits a broad maximum around 3.8 K, pointing to short-range ordering effects. Below 3 K, the susceptibility measured for $H = 1$ kOe (see lower curve in Figure 3, inset) behaves monotonically, showing no clear signature of the magnetic phase transitions observed below in the heat capacity and neutron diffraction data. Such an overall behavior of $\chi(T)$ is quite typical of systems exhibiting low-dimensional magnetic correlations, in which significant short-range magnetic ordering establishes at temperatures above the transition to long-range ordering.[13,14]

(11) Van Dyke, J. P. and Camp, W. P. *Phys. Rev. B* **1974**, *9*, 3121. Camp, W. P.; Van Dyke, J. P. *Phys. Rev. B* **1975**, *11*, 2579.
(12) Yamaji K., Kondo, J. *J. Phys. Soc. Jpn.* **1973**, *35*, 25.
(13) Feyerherm, R.; Loose, A.; Lawandy, M. A.; Li, J. *J. Phys. Chem. Solids* **2002**, *63*, 71.

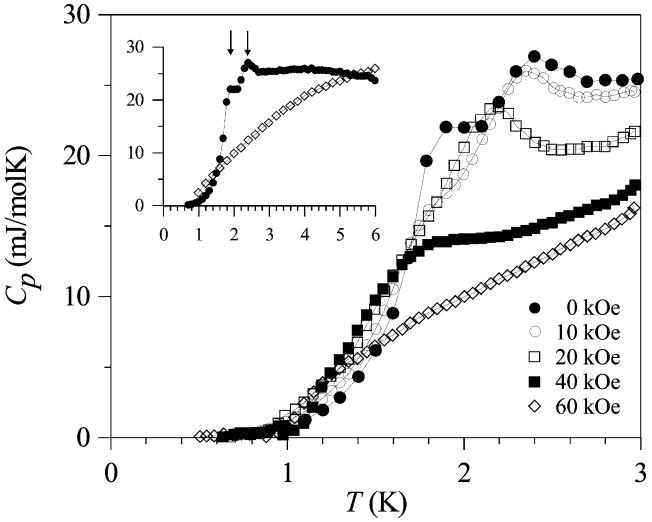

Figure 4. Specific heat of $Fe[C(CN)_3]_2$ at various external magnetic fields. The inset shows the data at 0 and 60 kOe in an extended temperature range. Arrows mark the two magnetic phase transitions.

As mentioned above, the magnetic topology of the $M[C(CN)_3]_2$ series is that of a 2D triangular lattice, where for M = Fe we expect Ising rather than Heisenberg behavior. To date, however, no theoretical formula describing the low-temperature behavior of the susceptibility of such a lattice has been derived. Analytical results on 2D lattices exist only for the cases of classical Heisenberg square and honeycomb lattices.[15,16] The present data qualitatively resemble the behavior calculated for these two cases which, however, cannot account for frustration effects expected for the triangular lattice. Fits using the theoretical expressions for the classical 1D Heisenberg or Ising chains, which would be valid in the case $J' \ll J$, did not give satisfactory results.

To obtain information on the T(H) phase diagram, additional magnetization measurements have been performed for various H values in the temperature region below 10 K; see the inset of Figure 3. For most measured data sets it remains hard to identify any magnetic transition below 2.5 K. Only for the data measured at H = 25 and 30 kOe kinks in the temperature dependence of the susceptibility allow one to identify magnetic transition temperatures of 2.2 and 2.0 K, respectively, for these field values. For H = 35 kOe, the transition is suppressed to below 1.8 K.

Heat Capacity. Figure 4 shows the specific heat of $Fe[C(CN)_3]_2$ measured between 0.6 and 6 K and in various values of the magnetic fields up to 60 kOe. In zero magnetic field, two anomalies around 1.9 and 2.4 K can be identified, indicating the presence of two magnetic phases. Application of a magnetic field leads to a suppression of both transitions. While the lower transition is suppressed already by a field of 20 kOe, the higher transition persists up to 40 kOe but is suppressed in a field of 60 kOe. The specific heat anomalies superimpose a high "background" which we associate with significant low-dimensional short-range ordering effects. These appear to dominate the specific heat at temperatures above the magnetic transitions and are also suppressed by application of a magnetic field (see Figure 4, inset). Because of the low quality of the data measured on the powder sample, we refrain from a more quantitative analysis.

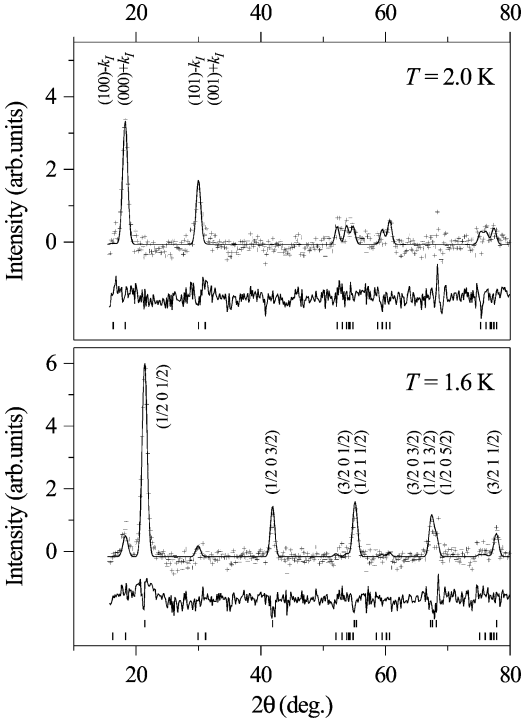

Figure 5. Difference diffractograms (+) taken at 2.0 and 1.6 K in zero magnetic field together with the Rietveld refinement of the corresponding magnetic structure models (solid line through the data) and the residual (solid line at the bottom). Vertical bars at the bottom mark the positions of allowed Bragg magnetic reflections. At 1.6 K the coexistence of both magnetic phases was assumed. The neutron wavelength was 4.513 Å.

Magnetic Ordering by Neutron Diffraction. To determine the magnetically ordered structures, high statistics neutron powder diffraction data were taken between 1.6 and 3 K in zero magnetic field. Figure 5 shows the difference of diffractograms measured at 2.0 and 2.9 K (top) and the difference of the 1.6 and 2.9 K diffractograms (bottom). Thus, only the additional Bragg reflections which are related to the magnetic ordering are visible. At 2.0 K, two significant magnetic Bragg reflections can be indexed only assuming an incommensurate magnetic propagation vector $k_I = (0.530(5)\ 0\ 0)$. At 1.6 K, the magnetic Bragg pattern is completely different. Several magnetic reflections can be identified and indexed by assuming a doubling of the unit cell along *a* and *c*, i.e., a propagation vector $k_{II} = (1/2\ 0\ 1/2)$. Obviously, the two phase transitions observed in the heat capacity data are related to two different magnetic phases, which in the following we will label I and II.

A Rietveld refinement of the 2.9 K diffractogram was performed by assuming the crystal structure parameters listed in Table 1. The only free parameters were scaling and line shape parameters. These were fixed in the subsequent refinement of the difference diffractograms. Thus, the only

(14) Bordallo, H. N.; Chapon, L.; Manson, J. L.; Hernández-Velasco, J.; Ravot, D.; Reiff, W. M.; Argyriou, D. N. *Phys. Rev. B* **2004**, *69*, 224405.
(15) Curely, J.; Lloret, F.; Julve, M. *Phys. Rev. B* **1998**, *58*, 11465. Curely, J.; Rouch, J. *Physica B* **1998**, *254*, 298. Curely, J. *Physica B* **1998**, *254*, 277.
(16) Maji, T. K.; Sain, S.; Mostafa, G.; Lu, T.-H.; Ribas, J.; Monfort, M.; Chaudhuri, N. R. *Inorg. Chem.* **2003**, *42*, 709.

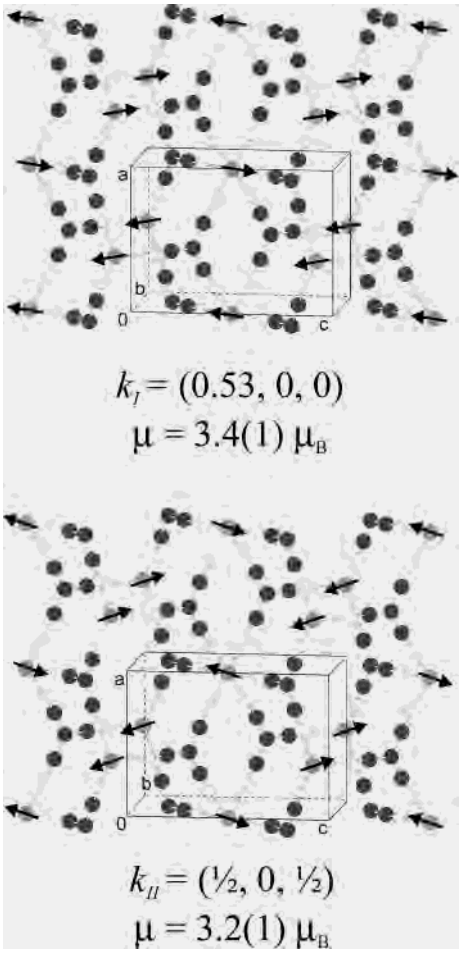

Figure 6. Two different magnetically ordered structures observed in $Fe[C(CN)_3]_2$. For the upper figure, k_I was approximated to (0.5 0 0). Note the different stacking of moments along the *c* axis. For clarity, only one of the two identical interpenetrating networks is shown. Moments at *y* and (*y* + 1), belonging to different networks, are oriented parallel in both structures.

free parameters in the latter refinements were the magnitude and direction of the ordered moment, the relative orientation of the moments in the two independent networks, and the propagation vector.

For phase I, we find best agreement between the measured and calculated relative intensities of the magnetic Bragg reflections by assuming an orientation of the ordered moment within the *bc* plane. Nearest-neighbor moments in the two independent networks are oriented parallel. The refinement results in an ordered moment $\mu = 3.4(1)\ \mu_B$ in phase I, with a sinusoidal modulation corresponding to the incommensurate k_I. A tilt of the moments from the *c* axis by $\alpha = 46(5)°$ toward *b* is determined, roughly parallel to the principal axes of the local Fe coordination octahedra located at $\alpha = 37°$ (see the first section). Note that the orientation of these axes alternates along c, resulting in a staggered moment arrangement.

For phase II, the refinement gives $\mu = 3.2(1)\ \mu_B$, again with the moment in the *bc* plane and parallel alignment between the two networks. Here, we find $\alpha = 63(5)°$. Hence, the transition between the two magnetic phases is associated with a slight reorientation of the ordered moments. In the 1.6 K difference diffractogram, a residual weak Bragg

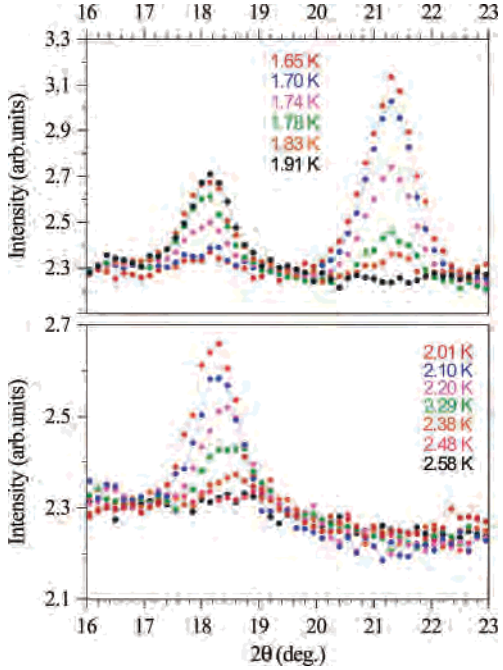

Figure 7. Low-angle section of neutron diffraction patterns measured between 1.7 and 2.5 K in zero magnetic field. The peak around 18° belongs to phase I, and the other peak around 21°, to phase II. The neutron wavelength was 4.513 Å.

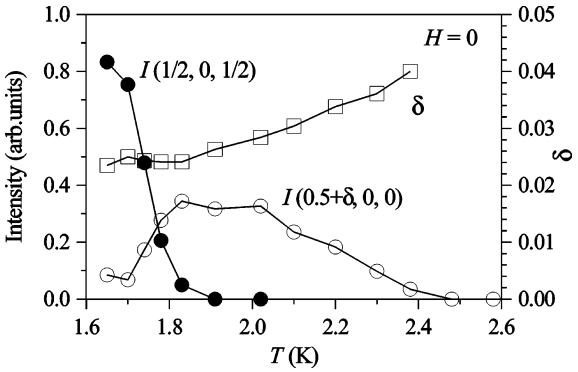

Figure 8. Zero-field temperature dependence of two Bragg peak intensities related to the two different magnetically ordered phases and of the incommensurate value of $k_{I,x}$.

reflection is observed around $2\theta = 18°$, pointing to a volume fraction of 20% of the sample that is still in phase I at this temperature. Figure 6 shows the two corresponding magnetic structures.

Figure 7 shows in more detail the development of the neutron diffraction data between 1.7 and 2.6 K. Above 2.0 K (see lower part of Figure 7), only Bragg reflections from phase I are present and vanish above around 2.4 K. A significant shift of the peak position to larger scattering angles is observed when increasing the temperature, reflecting a temperature dependence of the incommensurate propagation vector k_I. On cooling of the sample below 1.9 K, Bragg reflections from phase II appear with growing intensity, while the intensity of the reflections from phase I decreases.

Figure 8 shows the temperature dependence of the two Bragg peak intensities and of the value of $k_{I,x}$. The observed shift of the peak position between 2.0 and 2.4 K corresponds to an increase of $k_{I,x}$ from 0.525(5) to 0.540(5).

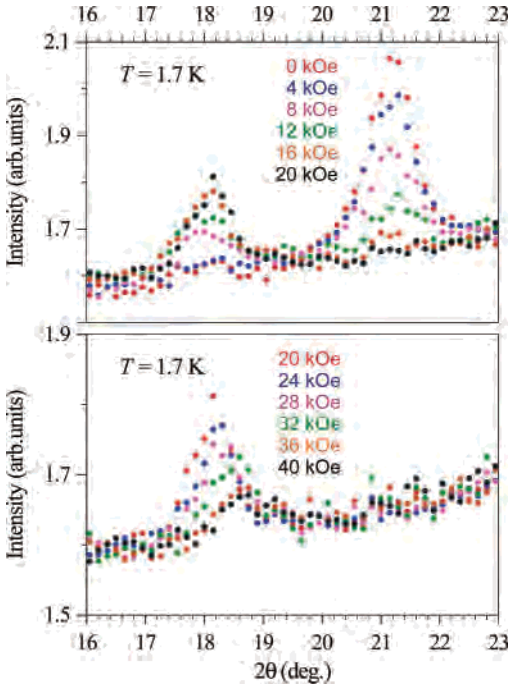

Figure 9. Low-angle section of neutron diffraction patterns measured at 1.7 K in external magnetic fields up to 40 kOe. The neutron wavelength was 4.513 Å.

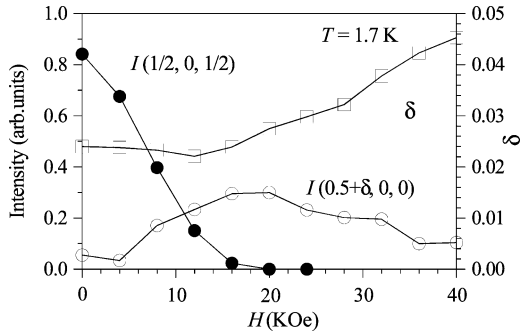

Figure 10. Magnetic field dependence of two Bragg peak intensities related to the two different magnetically ordered phases and of the incommensurate value of $k_{I,x}$.

Figure 9 shows the behavior at 1.7 K in the horizontal external magnetic field (field roughly parallel to the scattering vectors). Figure 10 shows the magnetic field dependence of the two Bragg peak intensities and of the value of $k_{I,x}$. Phase II is suppressed in a magnetic field of about 18 kOe and at the same time the sample switches to phase I. A further increase of the magnetic field leads to a suppression also of phase I, associated with an increase of the incommensurate value of $k_{I,x}$. However, a magnetic field of 40 kOe—the largest applicable in the experiment—is not sufficient to destroy phase I completely. These findings are roughly consistent with the specific heat data. Additional field-dependent neutron diffraction data taken at 2.0 K (not shown) show a suppression of phase I by a field of 25 kOe at this temperature.

Discussion

The temperature dependence of the magnetic susceptibility of $Fe[C(CN)_3]_2$ clearly indicates the dominance of 2D magnetic interactions. Significant short-range ordering takes place already above $T_{N,I} = 2.45$ K, leading to the susceptibility maximum at 3.8 K. The picture of a high degree of short-range ordering above $T_{N,I}$ is also supported by the zero-field heat capacity data. Because of this high degree of short-range ordering, the long-range magnetic ordering, taking place below $T_{N,I}$, is hardly visible in the susceptibility data. The short-range ordering is suppressed by large magnetic fields, as demonstrated by the heat capacity data and the suppression of the bump in the $\chi(T)$ curves.

The present magnetization, heat capacity, and neutron diffraction data allow one to construct the $T(H)$ magnetic phase diagram for $Fe[C(CN)_3]_2$, which is shown in Figure 11. Two different magnetic phases are observed, with phase II, embedded in phase I, being more stable for $T < 1.85$ K and for magnetic fields below about 20 kOe.

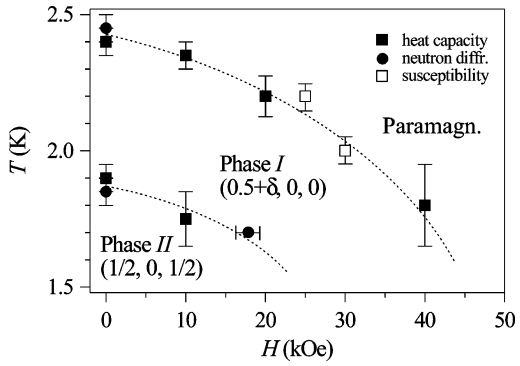

Figure 11. Magnetic phase diagram of $Fe[C(CN)_3]_2$ derived from the different experimental techniques employed in this work. The dashed lines are guides to the eye.

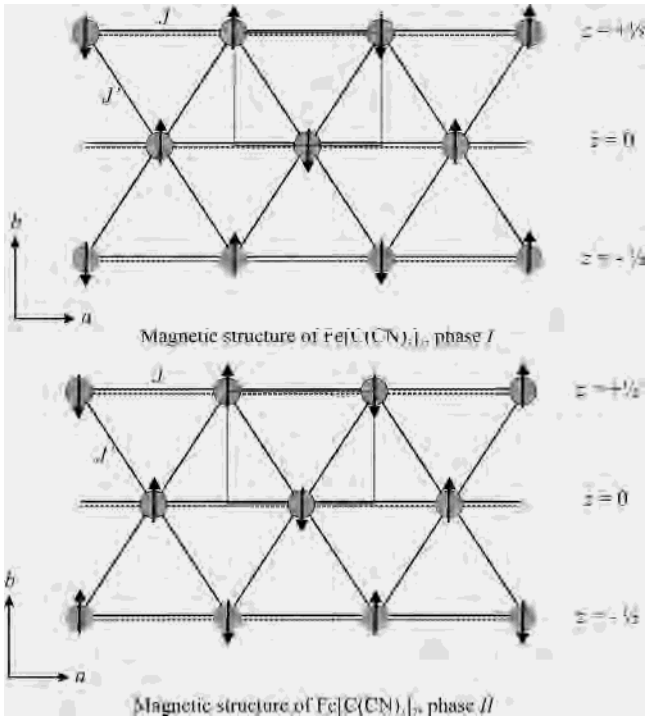

Figure 12. Projection of the magnetic structures of the two different ordered phases observed in $Fe[C(CN)_3]_2$ onto the ab plane (compare Figure 2). For clarity, the propagation vector of phase I is approximated as (0.5 0 0); i.e., the slow modulation of the moment magnitude along the a axis is omitted.

Table 2. Comparison of the Magnetic Behavior in the Series M[C(CN)$_3$]$_2$

M	T_N (K)	μ_{ord} (μ_B)	prop vector k	B_c (T)	moment orientation	ref
V	<1.7					5
Cr	6.1	4.7	($^1/_2$ $^1/_2$ 0)	?	$\mu \parallel c$	5
Mn	1.18	4.7	(0.622 0 0) $b' = 2b$	4.2	$\mu \parallel ab$ plane, spiral	7
Fe	2.45	3.4	(0.53 0 0)	2.5	$\mu \parallel bc$ plane, 45° from c, modulated	this work
	1.9	3.2	($^1/_2$ 0 $^1/_2$)	~6	$\mu \parallel bc$ plane, 63° from c	
Co	0.9	?	incommens	0.35	?	13
Ni	<0.5					13

Apparently, the two magnetically ordered phases are very close in energy. In Figure 12 we compare the ordered structures projected onto the *ab* plane. If one approximates $k_{I,x}$ with (0.5 0 0), the main difference between the two ordered phases is the relative arrangement of moments at (x, y, z) and (x, $y + 1$, $z + 1$) which are parallel in phase I and antiparallel in phase II. Assuming that only the exchange paths J and J' exist, the two corresponding magnetic structures with propagation vectors ($^1/_2$ 0 0) and ($^1/_2$ 0 $^1/_2$) indeed are energetically equivalent, since in both cases the J' bonds are alternating ferro- and antiferromagnetic. Minor next-nearest neighbor interactions may stabilize one structure over the other, but the present results show that any such interaction is too small to effectively lift the near degeneracy of the two phases. Therefore, the transition from phase I to phase II on cooling may be interpreted as a variant of a lock-in transition from an incommensurate to a commensurate value of k_x.

Further, from the fact that the ($^1/_2$ 0 $^1/_2$) state is the ground state, we may conclude that $J > J'$ in Fe[C(CN)$_3$]$_2$. In the opposite case, ferromagnetic alignment of the moments along rows parallel to α and antiparallel alignment between the rows, i.e., a propagation vector (000), would be energetically favored.

We now turn to a comparison of the magnetic ordering of Fe[C(CN)$_3$]$_2$ with the behavior of the other members of the M[C(CN)$_3$]$_2$ series. To date, magnetic ordering has been only reported for M = Cr and Mn. To complement these studies, in the course of this work additional low-temperature heat capacity measurements on Ni[C(CN)$_3$]$_2$ and Co[C(CN)$_3$]$_2$ have been performed. While in the Ni compound no indication for any phase transition was observed down to 0.4 K, a clear λ-type anomaly at 0.9 K observed in the Co compound indicated long-range magnetic ordering below that temperature. The heat capacity anomaly in Co[C(CN)$_3$]$_2$ is suppressed by magnetic fields larger than $H_c = 3.5$ kOe. Preliminary neutron diffraction data revealed the presence of several additional Bragg reflections below 0.9 K. These reflections could be indexed neither on the basis of the crystallographic cell nor assuming various kinds of doublings of the unit cell. Therefore, we assume that Co[C(CN)$_3$]$_2$ exhibits complex incommensurate ordering below 0.9 K.[17]

Table 2 lists the available information on the magnetic ordering of the M[C(CN)$_3$]$_2$ series for M = V, Cr, Mn, Fe, Co, and Ni. While no ordering is observed for the V and Ni compounds, the other members of the series order, each compound with a different kind of magnetic structure. The differences, however, are smaller than suggested by the different propagation vectors $\boldsymbol{k} = (k_a, k_b, k_c)$. We have discussed above that the two phases of the Fe compound with k_c values 0 and $^1/_2$ are almost degenerate. Further, a doubling of the unit cell along b, observed for M = Cr and Mn, is related to an antiparallel alignment of moments at y and ($y + 1$), belonging to the two *different* independent networks. In the M = Fe compound, this alignment is parallel. Besides this internetwork arrangement, within a *single* network the magnetic ordered structures observed for M = Cr, Mn, and Fe are indeed quite similar, with ka values ranging from 0.5 to 0.622.

In the work on Mn[C(CN)$_3$]$_2$[7] it was discussed in detail that incommensurate values of ka are expected for Heisenberg spins on "row model" triangular lattices. Here, the partial lifting of frustration—with $J' < J$ as in the Fe analogue—drives the value of k_a from 2/3 to somewhat smaller values. Ising-type single ion anisotropy, as expected for the Fe and Cr compounds, is expected to drive this value further toward a value of $^1/_2$. Indeed, the Cr and phase II of the Fe compound are driven to a commensurate state in this way. However, the anisotropy in the Fe compound is not strong enough to prevent the formation of an incommensurate state under the influence of an external magnetic field or by the action of thermal fluctuations.

Conclusion

We showed that the series M[C(CN)$_3$]$_2$, where M is a 3d transition metal, exhibits a quite rich magnetic behavior related to its distorted 2D triangular topology. Within this series, Fe[C(CN)$_3$]$_2$ is exceptional, exhibiting temperature- and field-dependent transitions between two different magnetically ordered phases, one of which is incommensurate. It remains to be clarified theoretically how the external magnetic field and thermal fluctuations stabilize one phase over the other and why these parameters influence the incommensurate magnetic propagation vector in the observed way. We are not aware of any report on other molecule-based triangular antiferromagnets. However, in view of the present results, more studies of such systems are desirable and will certainly be rewarding.

Acknowledgment. We thank M. Meissner and T. Polinski for performing the heat capacity measurements and T. Hauss and D. Toebbens for experimental support with the neutron diffraction experiments.

IC049423I

(17) Feyerherm, R.; Landsgesell, S. Hahn-Meitner-Institute and Berlin Neutron Scattering Center, Berlin, Germany. Unpublished data, 2003.